Available online at www.sciencedirect.com
SCIENCE DIRECT
International Journal of Mass Spectrometry 253 (2006) 87–97
International Journal of Mass Spectrometry
www.elsevier.com/locate/ijms

In situ petrographic thin section U–Pb dating of zircon, monazite, and titanite using laser ablation–MC–ICP-MS

Antonio Simonetti [a,*], Larry M. Heaman [a], Thomas Chacko [a], Neil R. Banerjee [a,b,1]

[a] *Department of Earth and Atmospheric Sciences, University of Alberta, 1-26 Earth Sciences Building, Edmonton, Alberta, Canada T6G 2E3*

[b] *Department of Earth Sciences, University of Bergen, Allegt. 41, 5007 Bergen, Norway*

Received 4 January 2006; received in revised form 1 March 2006; accepted 3 March 2006
Available online 4 April 2006

Abstract

A laser ablation–multiple collector–inductively coupled plasma mass spectrometry (LA–MC–ICP-MS) analytical protocol is used to date accessory minerals (zircon, monazite, and titanite) at high spatial resolution (5–40 μm) using standard petrographic thin sections. The MC–ICP-MS instrument is equipped with a modified collector array containing a combination of Faraday buckets and multiple ion counters, which produces accurate and precise geochronological data using small sample volumes (pit depth ≤2 μm at 5 μm and ≤15 μm at 40 μm spot sizes). Standardization and normalization factors for the $^{206}Pb/^{238}U$ and $^{207}Pb/^{235}U$ values are calculated based on well-characterized external mineral standards previously dated by high precision ID-TIMS analysis. During an analytical session, the 2σ relative standard deviation (i.e., external reproducibility) for the $^{206}Pb/^{238}U$ and $^{207}Pb/^{235}U$ values is ≤3%. The measured $^{207}Pb/^{206}Pb$ value is simultaneously corrected for instrumental mass bias by the aspiration of a Tl solution resulting in a 2σ relative standard deviation of between ∼0.3 and 1%. The accuracy of the analytical protocol was verified on petrographic thin sections of several samples previously dated by ID-TIMS. The capacity of this new, 'small volume' in situ dating technique to provide contextual, relatively rapid and accurate age information is a substantial improvement in reconnaissance-style studies of geological areas with scarce geochronological age information.

Keywords: Laser ablation; In situ U–Pb geochronology; MC–ICP-MS; Petrographic thin section

1. Introduction

Recent U–Pb isotope studies of accessory minerals (e.g., zircon, monazite) using laser ablation–(±multiple collector)–inductively coupled plasma mass spectrometry (LA–(± MC)–ICP-MS) have made significant advances in generating precise and accurate ages [e.g., Refs. 1–3]. Geochronological investigations of accessory minerals with LA–ICP-MS offer several advantages over other dating techniques. These include: (1) simple sample preparation procedures, (2) measurement of isotopic ratios at high spatial resolution (20–100 μm), (3) rapid analysis typically on the order of several minutes, and (4) low cost compared to other U–Pb analytical protocols, such as SHRIMP (sensitive high resolution ion microprobe) or ID-TIMS (isotope dilution-thermal ionization mass spectrometry). The coupling of laser ablation systems to magnetic sector, multiple collector–inductively coupled plasma mass spectrometry (MC–ICP-MS) technology has led to innovative research studies involving both stable and radiogenic isotope systems. These successes are due primarily to the overall high ionization efficiency of the ICP source, and simultaneous acquisition of ion beams with flat-topped peak shapes [e.g., Ref. 3]. Moreover, recent U–Pb laser ablation dating studies of zircon have been combined with in situ Hf isotope investigations on the same grain in order to provide additional information regarding the chemical nature of the host melts and hence their mantle or crustal source regions [e.g., Refs. 4–6]. The use of LA–MC–ICP-MS is also clearly advantageous when employed for certain research projects, such as dating a large population ($n > 50$) of detrital zircon grains in order to provide temporal limits for the ages of deposition and sources of provenance in orogenic terrains [e.g., Ref. 7].

* Corresponding author. Tel.: +1 780 492 4354; fax: +1 780 492 2030.
E-mail address: antonio.simonetti@ualberta.ca (A. Simonetti).
[1] Present address: Department of Earth Sciences, University of Western Ontario, London, Ontario, Canada N6A 5B7.

1387-3806/$ – see front matter © 2006 Elsevier B.V. All rights reserved.
doi:10.1016/j.ijms.2006.03.003

A recent technological innovation with MC–ICP-MS instrumentation for the purpose of in situ U–Pb investigations has been the design of a modified collector block containing a combination of Faraday collectors and ion counting detectors [3,8]. This modified collector block allows very low Pb ion signals (<1 mV) to be measured at high precision and thereby enables ablation experiments to be conducted using smaller sample volumes compared to those typically consumed for other LA–ICP-MS configurations (e.g., Refs. [2,9]). For example, a typical 30 s laser ablation analysis of zircon at 2 J/cm^2 energy density, 20–40 μm diameter, and 4 Hz produces a pit with a depth of ≤15 μm [3], which is markedly smaller than the thickness of a standard petrographic thin section (∼30 μm). In contrast, the laser ablation protocol outlined in Bence et al. [8] for in situ Pb isotope determinations of silicate glasses using a multiple ion counting system produces a pit depth of ∼65 μm (using a 93 μm spot size). The latter exceeds by a factor of ∼2 the thickness of a standard petrographic thin section, and consumes ∼20 times more sample material than the U–Pb laser ablation protocol for zircon described in Simonetti et al. [3]. The ability to date accessory minerals (e.g., zircon, monazite, titanite) in petrographic thin section with LA–MC–ICP-MS is advantageous in that it greatly reduces both sample preparation and analysis time relative to that needed for other geochronological techniques (e.g., in a typical 8-h analytical session, 3–5 thin sections with 10–20 spots per section can be analysed using the protocol outlined here). The technique also provides the opportunity to directly link age information for a particular sample with deformational fabrics, and pressure–temperature data derived from electron microprobe analysis in the same thin section. In situ U–Pb dating of monazite and zircon within petrographic thin section by LA–MC–ICP-MS has been previously conducted [e.g., Refs. 10,11]; however, in both studies the grains were ablated in 'raster' mode with typical sampling volumes of 80 μm × 18 μm × 5 μm [10] or 60 μm × 60 μm × 15 μm [11]. Employing such large raster areas on a routine basis limits the versatility of this technique, since many accessory minerals in thin section are not millimetric in size [e.g., 10], and many U-bearing grains of interest are heterogeneous containing fractures, mineral/fluid inclusions, regions of alteration and multiple age domains so it is advantageous to analyse the smallest volume possible. In addition, the previous studies of Foster et al. [10] and Zeh et al. [11] fail to provide the exact details on the methodology used to control the laser induced element fractionation (LIEF) for the Pb/U measurements of accessory minerals within petrographic thin sections. Finally, the LA–MC–ICP-MS methodology allows the analyses to be obtained at significantly lower cost (by a factor of 2–4) than is possible with either ID-TIMS or SHRIMP.

In this study, we report U–Pb age determinations for zircon, monazite, and titanite in standard petrographic thin sections using a MC–ICP-MS coupled to a frequency quintupled (λ = 213 nm) Nd:YAG laser ablation system. The accuracy and precision of the analytical protocols employed during this study are demonstrated by comparing the U–Pb ages of accessory minerals determined directly in petrographic thin sections to the age results previously obtained on these same samples by ID-TIMS.

2. Analytical techniques

2.1. Instrumentation

Isotopic data were acquired using a Nu Plasma MC–ICP-MS (Nu Instruments, UK) coupled to a UP213 laser ablation system (New Wave Research, USA). The MC–ICP-MS is equipped with a unique collector configuration consisting of 12 Faraday 'buckets' and three ion counters [3]. This configuration allows for simultaneous acquisition of ion signals ranging from mass ^{203}Tl to ^{238}U, with the ^{207}Pb, ^{206}Pb, and ^{204}Pb (+^{204}Hg) ion beams measured on the ion counting channels. The information regarding the nature of the ion counters, the calibration of the Faraday-ion counter biases (associated linearity), and data reduction protocol are described in detail in Simonetti et al. [3]. A summary of instrument parameters used for both the laser and MC–ICP-MS are listed in Table 1.

The ion counters consist of discrete dynode multipliers (manufactured by ETP) and ion signals are bent into the electron multiplier entrances using small deflectors. The latter offer a simple, but effective means of protecting the ion counters from excessive beams (typically >10^7 cps; counts per second) that may be incident on the devices. The multipliers can safely measure signals up to several (1–2) × 10^6 cps; however, ion signals were kept below 1 × 10^6 cps in almost all of the laser ablation analyses of zircon so as to prolong the longevity of the ETP detectors. The linearity and stability of the ion counters are better than 0.2% during any one analytical session, whereas dark

Table 1
Operating conditions and instrument settings

MC–ICP-MS	
Model	Nu plasma from Nu instruments
Forward power	1300 W
Reflected power	≤10 W
Cool gas flow rate	13 L min^{-1} (Ar)
Auxiliary gas flow rate	1 L min^{-1}(Ar)
Sample transport	
Ablation cell	1 L min^{-1}(He)
DSN-100	Membrane—3.00 to 3.50 L min^{-1}(Ar) heated to 110 °C, spray chamber—0.30 L min^{-1}(Ar) heated to 110 °C
Nebuliser—DSN	Glass expansion micromist (borosilicate glass)—100 μL min^{-1} equipped with Teflon PTFE adaptor and PFA Teflon tubing (1.3 mm OD × 0.25 mm ID)
Sampler cone	Ni with 1.15 mm orifice
Skimmer cone	Ni with 0.6 mm orifice
Laser	
Model	UP213 Nd:YAG—new wave research with aperture imaging system
Wavelength	213 nm
Maximum output energy	3 mJ per pulse at 20 Hz using a 160 μm spot size
Pulse width	3 ns
Energy density	2–3 J/cm^2
Focus	Fixed at sample surface
Repetition rate	4 Hz
Spot size	Single spot analysis—5, 20, 30, 40 μm

noise is 0.1 cps or better. At the start of each analytical session, the Faraday-ion counter bias is determined using a mixed 0.4 ppb standard solution of Pb (NIST SRM 981) and Tl (NIST SRM 997). The Faraday-multiplier calibration is calculated using a two sequence acquisition, where the $^{207}Pb/^{206}Pb$ [=0.914585] [12] is measured on the IC1 (ion counter #1)–L3 (Faraday) combination. The IC0 (ion counter #0) and IC2 (ion counter #2) calibrations are determined against the IC1 bias using the measured $^{207}Pb/^{206}Pb$ and $^{206}Pb/^{204}Pb$ [=16.9356] [12] values, respectively. This approach is similar to that adopted in previous isotopic studies involving MC–ICP-MS instruments equipped with multiple ion-counting devices [13]. Correction for LIEF and possible instrumental drift during a single laser ablation session of unknowns using the Tl-doping method was achieved by analysis of the matrix-matched 'external' zircon (BR266), monazite (Western Australia), and titanite (Khan) standards described below. The measured Pb/U values for the unknowns are compared to those obtained for their respective standards (ablated using identical run conditions) at the start of an analytical session, and normalization (=measured value/'true' value) factors are determined.

2.2. Measurement protocol

A routine U–Pb analysis consists of a 30 s blank measurement prior to the commencement of the laser ablation. The ablated particles are transported into the sample-out line with a He carrier gas and mixed with nebulized thallium (Saint-Gobain Tygon® tubing) via a 'Y'-connection located just prior to the torch box. The simultaneous introduction of laser-induced and dried solution aerosols was developed several years ago as an alternative calibration method for various laser ablation–ICP-MS instruments [e.g., Refs. 14,15]. A NIST SRM 997 thallium isotopic standard solution (1 ppb 2% HNO_3) is nebulized using a DSN-100 desolvating introduction system (Nu Instruments, UK) and aspirated (free aspiration mode) into the ICP source during the laser ablation run. Both the spray chamber and desolvating membrane of the DSN-100 are heated to 110 °C, with the Ar (Argon) flow rate set to 0.3 L min^{-1} and 3.0–3.5 L min^{-1} for the spray chamber and desolvating membrane, respectively. The measured Pb/U values are positively correlated with the membrane gas flow rate [3], and this is an expected result since varying the mixture of He and Ar within the main sample-out tube will most certainly change the plasma characteristics [e.g., Refs. 16,17]. The DSN membrane (Ar) flow rate was set so as to produce a measured $^{206}Pb/^{238}U$ value close to the external mineral standard's 'true' value during the laser ablation runs (also minimizes the normalization correction). The measured $^{205}Tl/^{203}Tl$ value is used to correct the measured Pb isotope ratios for instrumental mass bias using the reference value of 2.3871 [18]. The analytical protocol adopted here involving a Tl-doping method for monitoring of instrumental mass bias yields 2σ relative standard deviations that are ≤1% ($^{207}Pb/^{206}Pb$) and ≤3% ($^{206}Pb/^{238}U$, and $^{207}Pb/^{235}U$). Details of the measurement routine used in this study are described in Simonetti et al. [3]. The main difference to this procedure is the method used in this study for monitoring primarily the Pb/U values. For epoxy grain mounts, internal zircon standard and unknown zircon grains are placed together so that the standard can be frequently analysed without opening-up the ablation cell (typically after every 10–12 unknowns). In contrast, the normalization factors for the $^{206}Pb/^{238}U$ and $^{207}Pb/^{235}U$ values for age determinations of accessory minerals in thin section were determined at the start of each analytical session using appropriate matrix-matched external mineral standards (described below) that have previously been accurately dated by ID-TIMS. In addition, the variation in the measured Pb/U values was monitored on several days by analysis of the external standard at both the beginning and end of an ~8 h long analytical session. The plasma was permitted to re-equilibrate with the ablation cell during a 15 min period subsequent each thin section exchange. Despite the fact that the laser ablation cell is opened on several occasions during one analytical session in order to permit the exchange of thin sections, the Pb/U values changed by <3%, which is smaller than the 2σ relative standard deviation (i.e., external reproducibility) associated with the Tl-doping analytical protocol employed here [3].

3. Results and discussion

3.1. Zircon

The well-calibrated international zircon standard BR266 was used as the external standard for the normalization of the Pb/U values and verification of the $^{207}Pb/^{206}Pb$. Stern and Amelin [19] report 22 new ID-TIMS ages based on randomly selected fragments of BR266, and these yielded weighted mean $^{206}Pb/^{238}U$ and $^{207}Pb/^{206}Pb$ ages of 559.0 ± 0.2 Ma and 562.6 ± 0.2 Ma, respectively. The BR266 fragment used here yielded a highly precise and accurate laser ablation–MC–ICP-MS weighted average $^{207}Pb/^{206}Pb$ age of 564.7 ± 1.9 Ma (2σ, n = 15 analyses; Simonetti et al. [3]), which is indistinguishable from the ID-TIMS $^{207}Pb/^{206}Pb$ age of 562.6 ± 0.2 Ma.

A thin section from sample LH94-15, a homogeneous calc-alkaline enderbite was investigated in this study. The crystal morphology of the zircons in this sample implies an igneous derivation [20]. A previous ID-TIMS investigation yielded an age of 1830 ± 2 Ma (2σ), and is interpreted as the crystallization age of this enderbite [20]. Due to their homogeneous nature, abundant Pb (~100 ppm) and U (~300 ppm) contents, and precise ID-TIMS age determination, zircons from sample LH94-15 were adopted as the 'internal' standard in our previous U–Pb laser ablation study [3]. Repeated analysis of zircons from LH94-15 over a period of several months by different analysts yielded highly reproducible results with ages of 1830 ± 6.7 Ma, 1826 ± 6 Ma, and 1827.9 ± 6.1 Ma (2σ; [3]), that are indistinguishable from the ID-TIMS concordant age of 1830 ± 2 Ma (2σ). A large single zircon from a thin section of sample LH94-15 was ablated 10 times consecutively using a spot size of 40 μm (inset of Fig. 1). The U–Pb isotope data are listed in Table 2 and shown in a concordia plot (Fig. 1). All 10 analyses are concordant and combine to yield an accurate concordia age of 1835.7 ± 4.7 Ma (2σ), which is indistinguishable from the ID-TIMS age of 1830 ± 2 Ma [20]. The individual spot analyses yield uniform $^{207}Pb/^{206}Pb$ ages (1813–1834 Ma) despite a

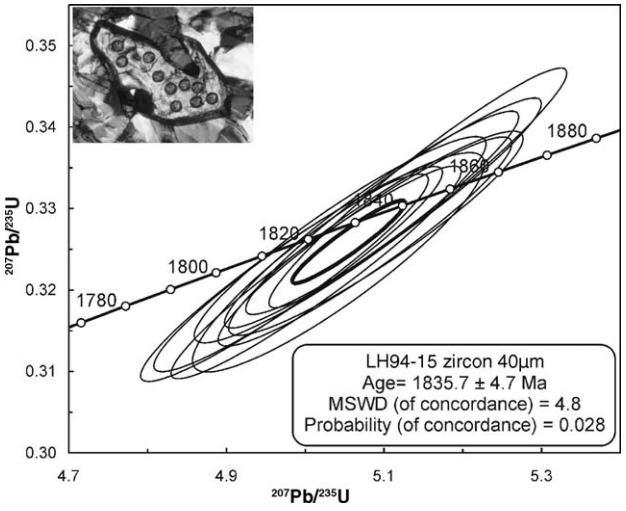

Fig. 1. Concordia diagram illustrating the U–Pb laser ablation results for 10 analyses of a zircon grain within a petrographic thin section of an enderbitic sample from the Jan Lake Complex. Inset displays the locations of the 40 μm spots within the grain, and is surrounded by predominantly pyroxene, plagioclase, biotite and quartz. This plot and subsequent concordia diagrams were constructed with Isoplot version 3.0 [33]. Error ellipses are at 2σ levels.

rather large range in ^{206}Pb ion signal intensities (from ~130,000 to ~400,000 cps; Table 2). The amount of ^{204}Pb measured in the individual laser ablation runs was always <13 cps (Table 2) attesting to the 'clean' nature (extremely low common Pb content) of the zircon grain. In order to provide the best comparison between the laser ablation data versus the ID-TIMS results for the same samples, the correlation coefficients ('rho' values) for the ^{207}Pb/^{235}U and ^{206}Pb/^{238}U values listed in Table 2 were calculated according to the equations defined in Ludwig [21].

Zircons in a thin section of sample TL40, the Tallan Lake granodiorite from the Grenville Province in southeastern Ontario, Canada [22] were also investigated here as an additional test of the accuracy of the analytical protocol. A previous ID-TIMS investigation of four zircon fractions from sample TL40 yielded a discordia line (97% probability of fit) with an upper intercept age of 1254 +23/−4 Ma (2σ) [22]. The four zircon fractions are characterized by Pb and U concentrations of ~80 ppm and ~330–400 ppm, respectively, and common Pb contents from 10 to 91 pg [22]. The upper intercept age of 1254 Ma is interpreted as representing the time of zircon crystallization during the emplacement of the granodiorite. In addition, the selected zircon fractions did not show any evidence of a ~1020 Ma hydrothermal event that disturbed the Rb–Sr isotope system in parts of this granodiorite along discrete fractures [22].

Using spot sizes of 20, 30, and 40 μm, 24 analyses were conducted on six different zircon grains in one thin section of sample TL40 (Table 2). The zircon standard BR266 was used for the external normalization of the Pb/U values at identical spot sizes of 20, 30, and 40 μm. The data are illustrated in several concordia diagrams (Fig. 2(A)–(D)). The three upper intercept ^{207}Pb/^{206}Pb ages based on the most concordant analyses for each of the three different spot sizes are 1249.2 ± 8.4 Ma (2σ: 40 μm; six analyses), 1258 ± 21 Ma (2σ: 30 μm; six analyses), and 1234 ± 28 Ma (2σ: 20 μm; six analyses). These ages are statistically indistinguishable from one another and from the upper intercept ID-TIMS age of 1254 +23/−4 Ma [22]. An upper intercept ^{207}Pb/^{206}Pb age of 1250.1 ± 9.1 Ma (2σ) is obtained when the 18 analyses from the different spot sizes are compiled, which is again indistinguishable to the previously published ID-TIMS age. It should be noted that the use of a 40 μm spot size yields a more precise age than those obtained with the smaller spot sizes of 20 and 30 μm, and that the degree of Pb/U fractionation is negatively correlated with spot size. This inverse relationship between the ^{206}Pb/^{238}U inter-element fractionation and spot size is in agreement with previous studies based on laser ablation results of the NIST 612 international glass standard [16,23]. It should also be noted that, despite any pre-selection of optimal zircon grains in the thin section or the possible incorporation of radiation damaged areas in the analytical spots, the LA–MC–ICP-MS results show no detectable dispersion of the data towards the ~1020 Ma age of hydrothermal activity that locally affected this granodiorite outcrop. As a consequence, the LA–MC–ICP-MS data, like the TIMS data, provides an accurate indication of the igneous crystallization age of the granodiorite.

3.2. Monazite

A monazite grain sampled from an alluvial placer deposit located within the Eleys Creek region of the Shaw River Ta/Sn-bearing pegmatites, NW district of Western Australia (provided by A. Mariano) was used as the external standard for this study. The pegmatites are emplaced within the Archean Pilbara craton, and the monazite yields a concordant ID-TIMS age of 2842.9 ± 0.3 Ma (Table 3; Heaman et al., Unpublished data). The Western Australia monazite external standard is characterized by U, Th, and Pb contents of 1424, 23565, and 3970 ppm, respectively. The U–Pb laser ablation analyses of the western Australian external monazite standard were bracketed and normalized with another monazite (from Madagascar) that has also been dated by ID-TIMS (512.7 ± 1.8 Ma; Heaman et al., Unpublished data). U–Pb laser ablation results (n = 8 analyses) for the Western Australia monazite using a spot size of 12 μm yielded a concordant age of 2843.7 ± 6.5 Ma that is indistinguishable from the ID-TIMS age.

At the start of an analytical session, analyses of the monazite standard were conducted using the same instrument settings as those used subsequently for the petrographic thin sections: 4 Hz repetition rate, ~3 J/cm^2 and spot size of 5 μm. We investigated three monazite grains from two different thin sections for sample LH94-11a, which is the leucosome component of a migmatitic meta-graywacke from the Jan Lake Complex, Saskatchewan, Canada (Ashton et al. [20]). A 5 μm spot size was used for the analyses because of the extremely high concentrations of both Pb and U, which range between 1000 and 6000 ppm for each element [20]. The results are listed in Table 3 and shown in Fig. 3. With the exception of one analysis (grain 2–3; Table 3), none of the analyses detected the presence of any common Pb.

Ashton et al. [20] report seven single-grain near-concordant monazite U–Pb ages determined by ID-TIMS that range from

Table 2
U–Pb laser ablation and ID-TIMS results for zircon from samples LH94-15 and TL40

Anal. #	^{204}Pb (cps)	^{206}Pb (cps)	^{207}Pb/^{206}Pb	±2σ	^{207}Pb/^{235}U	±2σ	^{206}Pb/^{238}U	±2σ	Rho value	^{207}Pb/^{206}Pb (Ma)	±2σ (Ma)
LH94-15											
ID-TIMS[a]			0.11187	0.00012	5.0545	0.024	0.3277	0.0012		1830	2
1-40 μm	0	260333	0.11158	0.00125	5.143	0.154	0.3325	0.0120	0.96	1825	20
2-40 μm	13	195729	0.11184	0.00168	5.042	0.151	0.3234	0.0110	0.90	1830	27
3-40 μm	6.7	164720	0.11166	0.00128	5.089	0.153	0.3270	0.0102	0.93	1827	21
4-40 μm	5.6	155091	0.11082	0.00129	5.045	0.151	0.3262	0.0103	0.93	1813	21
5-40 μm	0.4	304299	0.11102	0.00117	5.085	0.153	0.3286	0.0109	0.95	1816	19
6-40 μm	0	160449	0.11175	0.00123	5.076	0.152	0.3259	0.0105	0.94	1828	20
7-40 μm	0	235855	0.11110	0.00118	4.991	0.149	0.3226	0.0103	0.94	1817	19
8-40 μm	0	131322	0.11210	0.00117	5.014	0.151	0.3222	0.0107	0.95	1834	19
9-40 μm	0	383834	0.11131	0.00114	5.112	0.153	0.3303	0.0109	0.95	1821	19
10-40 μm	11.9	211032	0.11098	0.00117	4.974	0.149	0.3215	0.0104	0.95	1816	19
TL40											
ID-TIMS[b]			0.08205	0.000040	2.3965	0.0060	0.2118	0.00053		1254	+23/−4
1a-40 μm	0	201757	0.08255	0.00089	2.181	0.066	0.1914	0.0067	0.96	1259	21
1b-40 μm	0	130083	0.08075	0.00090	2.046	0.061	0.1830	0.0066	0.96	1215	22
1c-40 μm	0	230976	0.08254	0.00088	2.177	0.065	0.1914	0.0073	0.98	1258	21
1d-40 μm	0	226418	0.08168	0.00089	2.121	0.064	0.1878	0.0063	0.95	1238	21
2a-40 μm	0	172301	0.08247	0.00092	2.159	0.065	0.1899	0.0065	0.95	1257	22
4a-40 μm	0	213708	0.07827	0.00098	1.789	0.054	0.1660	0.0052	0.92	1154	25
6a-40 μm	0	461793	0.08151	0.00085	2.143	0.064	0.1906	0.0068	0.97	1234	20
6b-40 μm	0	411367	0.08188	0.00085	2.096	0.063	0.1858	0.0068	0.97	1243	20
1e-30 μm	0	75263	0.08321	0.00098	2.259	0.068	0.1981	0.0072	0.95	1274	23
1f-30 μm	0	91668	0.08320	0.00093	2.273	0.068	0.1993	0.0075	0.97	1274	22
1g-30 μm	0	57286	0.07817	0.00110	2.095	0.063	0.1957	0.0063	0.90	1151	28
2b-30 μm	0	97493	0.08363	0.00097	2.271	0.068	0.1974	0.0069	0.95	1284	23
2c-30 μm	23	44789	0.08255	0.00215	2.275	0.068	0.2000	0.0063	0.64	1259	51
3a-30 μm	177	99146	0.08320	0.00225	2.273	0.068	0.1998	0.0071	0.67	1274	53
4b-30 μm	0	91245	0.07886	0.00089	2.018	0.061	0.1860	0.0069	0.97	1169	22
5-30 μm	0	115260	0.08153	0.00091	2.158	0.065	0.1927	0.0073	0.97	1234	22
6c-30 μm	0	83153	0.07989	0.00102	2.051	0.062	0.1871	0.0076	0.98	1194	25
6d-30 μm	0	136812	0.07983	0.00091	2.188	0.066	0.1995	0.0085	0.71	1193	22
1h-20 μm	0.9	26782	0.08152	0.00137	2.260	0.068	0.2034	0.0089	0.96	1234	33
1i-20 μm	8	34057	0.08191	0.00146	2.283	0.069	0.2038	0.0078	0.89	1243	35
2d-20 μm	10.9	36275	0.08366	0.00154	2.298	0.069	0.1998	0.0070	0.85	1285	36
3b-20 μm	106	32686	0.08199	0.00348	2.189	0.066	0.1941	0.0073	0.23	1245	83
6e-20 μm	1.5	13402	0.08140	0.00239	2.063	0.062	0.1865	0.0068	0.63	1231	58
6f-20 μm	0	43914	0.08179	0.00132	2.278	0.068	0.2029	0.0073	0.90	1241	32

[a] Average of three ID-TIMS analyses from Ashton et al. [20].
[b] Average of four ID-TIMS analyses and upper intercept age (Heaman et al. [22]).

1802 to 1815 Ma. These monazite dates are consistent with a well-known 1790–1810 Ma Paleoproterozoic thermal event that affected the region. Monazite grain #1 from thin section #1 yielded an upper intercept ^{207}Pb/^{206}Pb age of 1801.4 ± 8.4 Ma (2σ), which falls within the range of monazite ID-TIMS dates reported for this sample [20]. Fig. 3(A) shows that with the exception of one reversely discordant analysis, the remaining data points are either concordant or near-concordant. A single monazite grain analysed in thin section #2 yielded slightly less concordant data but an identical upper intercept age of ^{207}Pb/^{206}Pb age of 1803.5 ± 7.8 Ma (Fig. 3(C)). Analyses of a second monazite grain from thin section #1 indicate a more complex history that is reflected in both the core-rim compositional domains revealed in a back scattered electron image (Fig. 3(D)), and the large range in ^{207}Pb/^{206}Pb ages between 1807 and 2435 Ma (Table 3). Five analyses of this grain gave results that were very similar to those obtained for grain #1 in this section (Fig. 3(B)). However, three analyses near the core of grain #2 yielded a much older average ^{207}Pb/^{206}Pb age of 2428 ± 11 Ma (2σ; Table 3). A discordia line constructed to pass through all analyses yields an upper intercept age of 2502 ± 64 Ma (2σ) and a lower intercept age of 1727 ± 52 Ma (2σ; Fig. 3(B)). It is important to note that the older monazite age population was not detected in the ID-TIMS study of this sample and highlights an advantage of this in situ technique. The older U–Pb monazite core analyses obtained here agree with the timing of an older metamorphic/plutonic event previously determined from other units within the Jan Lake Complex (e.g., the 2450 ± 8 Ma Sahli granite; Ashton et al. [20]). Thus, the older age population of monazite in LH94-11a may record an earlier period of metamorphism experienced by this sample that was broadly coeval with the intrusion of high-temperature magmas in the region. Alternatively, the older monazite core may be detrital in origin and reflect the age of one of the source rocks that

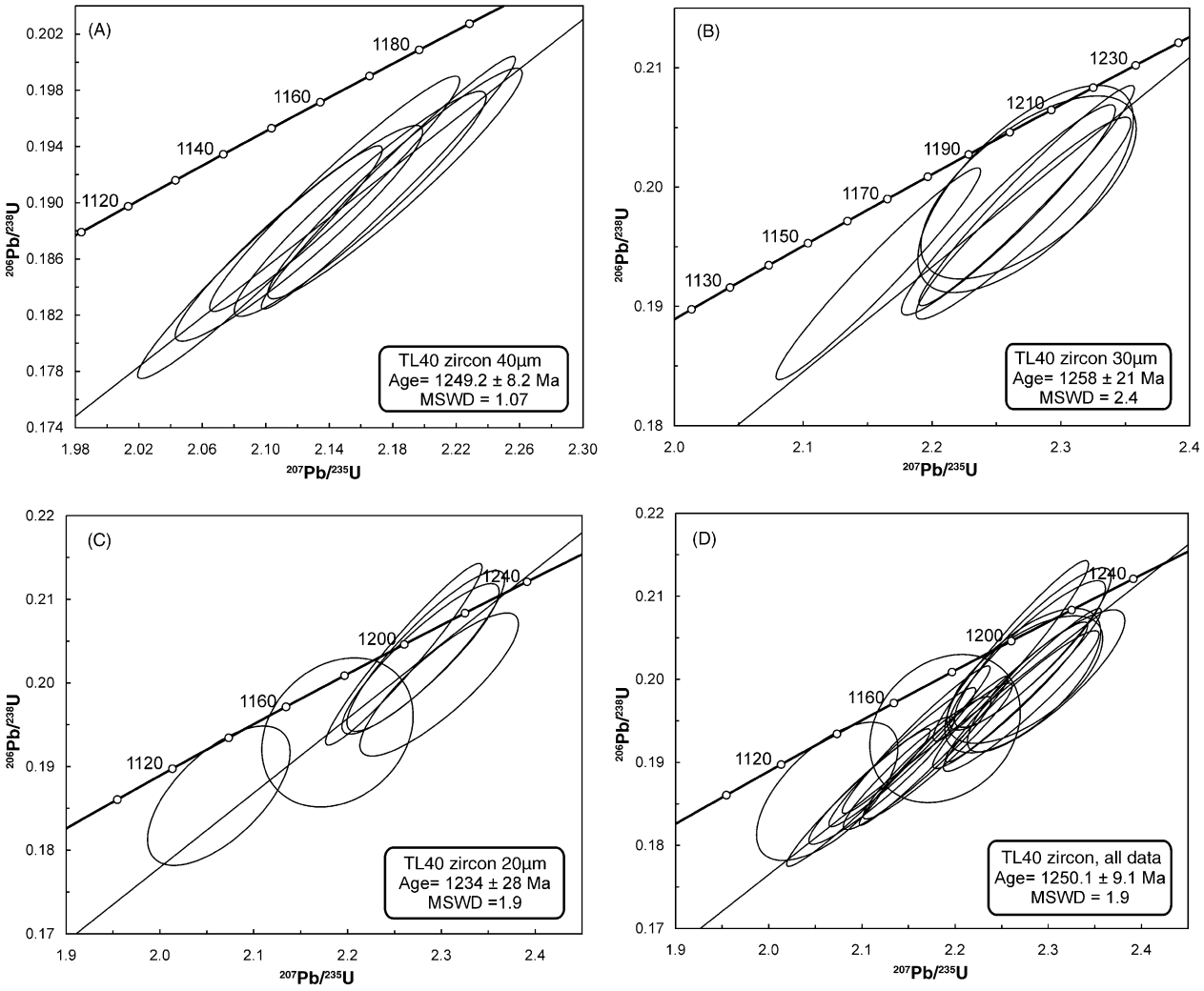

Fig. 2. U–Pb laser ablation results of various zircon grains within a petrographic thin section of granodiorite sample TL40 using variable spot sizes of (A) 40 μm, (B) 30 μm, and (C) 20 μm. (D) A compilation concordia diagram that combines all the data from the various spot sizes. Error ellipses are at 2σ levels.

provided detritus to the sedimentary precursor of sample LH94-11a. The preservation of a ca. 2450 Ma monazite core in a sample that experienced upper amphibolite-facies metamorphism at ca. 1800 Ma is consistent with the experimental data of Cherniak et al. [24], which indicate that Pb diffusivity in monazite is comparable to that in zircon. This exceedingly slow rate of Pb diffusion in monazite is also corroborated by a number of recent studies of high-grade metamorphic rocks. In particular, Schmitz and Bowring [25] reported the preservation of pre- or early metamorphic monazites (ca. 2770 Ma) in lower crustal xenoliths that experienced ultra-high-temperature metamorphism (>1000 °C) at ca. 2720 Ma. Similarly, Bosch et al. [26] report the preservation of detrital monazite ages (ca. 1360 Ma) in pelitic rocks that experienced granulite-grade metamorphism (∼850 °C) at ca. 1085 Ma.

It is important to note that the ability to conduct U–Pb laser ablation analysis of monazite at a spatial resolution of 5 μm makes it possible to document in detail discrete U–Pb ages within a single complex multi-age grain. Such complex monazite growth histories may be undetectable or obscured in isotopic analyses of entire monazite grains, or by rastering over much larger areas within individual grains during laser ablation–ICP-MS analysis.

3.3. Titanite

Titanite typically contains significant quantities of common Pb, therefore the accuracy of U–Pb dates obtained from titanite is critically dependent on the correct assessment of the common Pb component. Here we adopt a method used for the common Pb correction of perovskite, that involves using the line projected through the uncorrected data on a Tera–Wasserburg diagram [27] to determine the common Pb-component (y-intercept) on the $^{207}Pb/^{206}Pb$ axis. The y-intercept value is then used to calculate the proportion of common Pb for each individual analysis using well established U–Th–Pb radiogenic decay equations [28]. The main assumption in the calculation is that the mineral being dated is concordant. This same methodology has also been adopted in a recent U–Pb dating of titanite by LA–ICP-MS [29]; however, in this study the titanite crystals were separated and placed within

Table 3
U–Pb laser ablation and ID-TIMS results for monazite from sample LH94-11a

Anal. #	^{204}Pb (cps)	^{206}Pb (cps)	^{207}Pb/^{206}Pb	±2σ	^{207}Pb/^{235}U	±2σ	^{206}Pb/^{238}U	±2σ	Rho value	^{207}Pb/^{206}Pb apparent age (Ma)	±2σ (Ma)
ID-TIMS[a]			0.11051	0.00012	4.905	0.022	0.3219	0.0012		1808.9	4
TS #1											
Grain 1-1	0	176220	0.11043	0.0012	5.376	0.161	0.3527	0.012	0.96	1806	20
Grain 1-2	0	176196	0.11030	0.0012	4.962	0.149	0.3269	0.011	0.95	1804	20
Grain 1-3	0	185472	0.11039	0.0012	4.741	0.142	0.3119	0.010	0.95	1806	19
Grain 1-4	0	184988	0.11017	0.0012	4.891	0.147	0.3218	0.010	0.94	1802	20
Grain 1-5	0	150403	0.11010	0.0019	4.812	0.145	0.3170	0.015	0.99	1801	32
Grain 1-6	0	144233	0.11022	0.0012	4.687	0.141	0.3088	0.010	0.94	1803	20
Grain 1-7	0	210101	0.10965	0.0012	4.963	0.149	0.3285	0.013	0.99	1794	20
Grain 2-1	0	192095	0.15796	0.0017	9.792	0.294	0.4500	0.014	0.94	2434	18
Grain 2-2	0	208179	0.15727	0.0017	9.548	0.287	0.4398	0.014	0.94	2426	18
Grain 2-3	556	223161	0.15806	0.0020	9.645	0.289	0.4462	0.014	0.92	2435	21
Grain 2-4	0	343575	0.11093	0.0012	4.897	0.147	0.3193	0.011	0.95	1815	19
Grain 2-5	0	379311	0.11343	0.0014	5.064	0.152	0.3254	0.010	0.92	1855	22
Grain 2-6	0	318913	0.12758	0.0018	6.155	0.185	0.3511	0.011	0.90	2065	24
Grain 2-7	0	436284	0.11163	0.0012	4.825	0.145	0.3131	0.010	0.95	1826	19
Grain2-8	0	298679	0.11044	0.0012	4.825	0.145	0.3176	0.010	0.94	1807	19
Grain 2-9	0	311166	0.11097	0.0012	4.816	0.145	0.3157	0.010	0.95	1815	19
TS #2											
Grain 1-1	0	271159	0.11095	0.0013	4.588	0.138	0.2999	0.0099	0.94	1815	21
Grain 1-2	0	262306	0.11005	0.0011	4.619	0.139	0.3048	0.0101	0.95	1800	19
Grain 1-3	0	252373	0.10992	0.0012	4.577	0.137	0.3031	0.0095	0.94	1798	19
Grain 1-4	0	171858	0.11045	0.0012	4.587	0.138	0.3009	0.0101	0.95	1807	19
Grain 1-5	0	238037	0.11041	0.0012	4.618	0.139	0.3039	0.0100	0.95	1806	19
Grain 1-6	0	228962	0.11034	0.0012	4.589	0.138	0.3015	0.0098	0.94	1805	20

[a] Average of six analyses from Ashton et al. [20].

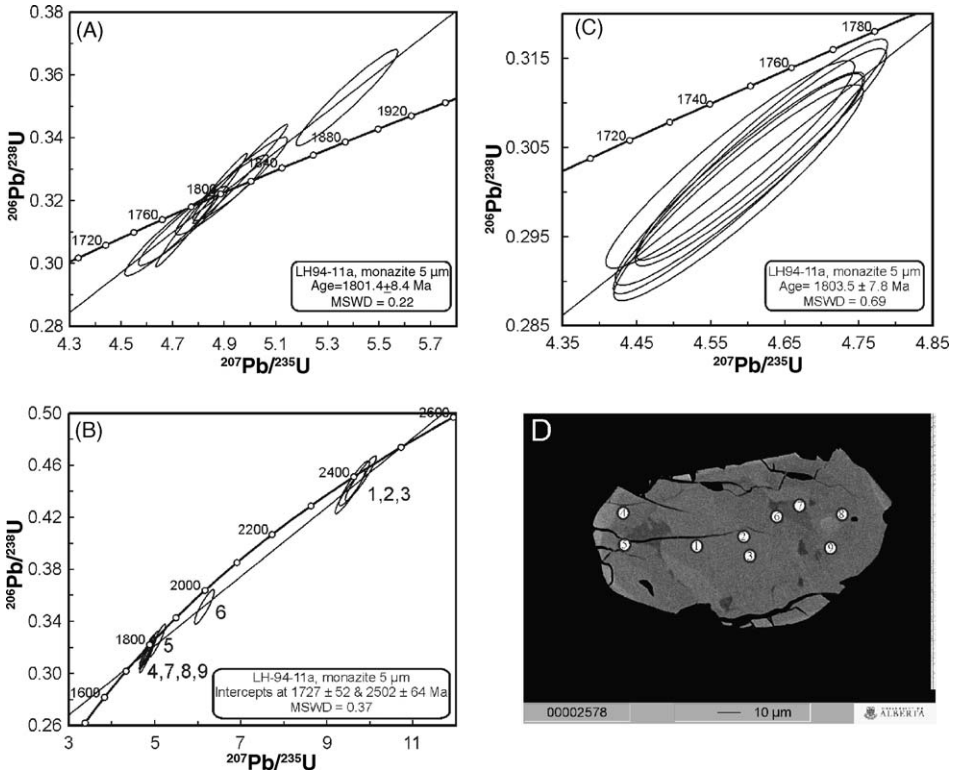

Fig. 3. (A) Concordia diagram illustrating the age determination for monazite grain #1 from thin section #1 of the leucosome from migmatitic paragneiss sample LH94-11a. (B) U–Pb laser ablation results for monazite grain #2 from thin section #1 for sample LH94-11a. The numbers alongside the ellipses correspond to laser pit locations shown in (D)—a back-scattered electron image of the monazite grain in question. (C) Concordia plot showing the age determination for monazite grain #1 from thin section #2 for sample LH94-11a. Error ellipses are at 2σ levels.

Table 4
U–Pb results for Coldwell complex and Khan titanites

Sample	^{206}Pb (cps)	Calculated ratios				% Rad. ^{206}Pb	Corrected ratios		Apparent ages (Ma)	
		^{238}U/^{206}Pb	±2σ	^{207}Pb/^{206}Pb	±2σ		^{206}Pb/^{238}U	±2σ	^{206}Pb/^{238}U	±2σ
Sample CL-2										
ID-TIMS[a]		5.3322	0.0133	0.07494	0.0003		0.1875	0.0005	1108	3
1	23460	4.4564	0.2291	0.2463	0.0400	80.3	0.1802	0.0115	1068	55
2	18533	4.9523	0.2285	0.1400	0.0064	92.7	0.1871	0.0093	1106	51
3	21738	5.0267	0.1728	0.1231	0.0030	94.7	0.1883	0.0068	1112	38
4	7773	4.6737	0.5326	0.1711	0.0055	89.1	0.1905	0.0244	1124	128
5	6824	4.3902	0.3723	0.2142	0.0083	84.0	0.1914	0.0193	1129	96
6	6461	5.4014	0.5149	0.1409	0.0035	92.6	0.1714	0.0176	1020	97
7	10379	4.9564	0.4104	0.1124	0.0024	95.9	0.1935	0.0167	1140	94
8	11361	4.5748	0.2681	0.1640	0.0110	89.9	0.1965	0.0128	1156	68
9	8971	5.3115	0.4970	0.1434	0.0054	92.3	0.1738	0.0176	1033	97
10	8799	4.7887	0.3080	0.1605	0.0165	90.3	0.1886	0.0134	1114	72
11	27092	5.1179	0.2829	0.1006	0.0021	97.3	0.1901	0.0108	1122	62
12	31037	5.2034	0.2271	0.1132	0.0031	95.8	0.1841	0.0084	1089	48
13	32318	4.9533	0.2144	0.1039	0.0015	96.9	0.1956	0.0087	1152	50
14	18008	4.8282	0.2011	0.1185	0.0030	95.2	0.1971	0.0086	1160	48
Sample CL-22										
ID-TIMS[b]		5.3625	0.0144	0.0764	0.0002		0.1865	0.0005	1102	3
15	22918	4.9995	0.2543	0.0916	0.0024	98.3	0.1967	0.0102	1157	59
16	38921	4.7574	0.2559	0.0988	0.0046	97.5	0.2049	0.0113	1202	65
17	239525	5.4034	0.2366	0.0849	0.0023	99.1	0.1834	0.0081	1086	48
18	31714	5.1161	0.2093	0.0849	0.0030	99.1	0.1937	0.0080	1141	47
19	105250	5.2759	0.3065	0.0804	0.0009	99.6	0.1888	0.0110	1115	65
Khan										
1	137887	12.2074	0.4826	0.0580	0.0008	100	0.0819	0.0032	507	20
2	153470	12.2271	0.4308	0.0577	0.0006	100	0.0818	0.0029	507	18
3	163834	12.2454	0.4216	0.0575	0.0015	100	0.0817	0.0028	506	17
4	156877	12.3739	0.4176	0.0578	0.0006	100	0.0808	0.0027	501	17
5	158549	12.1129	0.4085	0.0579	0.0007	100	0.0825	0.0028	511	17
6	165242	12.2019	0.4137	0.0570	0.0014	100	0.0820	0.0028	508	17
7	211956	11.7627	0.5294	0.0578	0.0006	100	0.0850	0.0038	526	24
8	244443	12.0223	0.4526	0.0585	0.0008	99.9	0.0831	0.0031	515	19
9	248100	12.0065	0.4393	0.0579	0.0007	100	0.0833	0.0030	516	19
10	255316	11.8615	0.4817	0.0589	0.0010	99.9	0.0842	0.0034	521	21
11	264936	11.6380	0.3912	0.0576	0.0007	100	0.0859	0.0029	531	18
12	269623	11.9719	0.4356	0.0577	0.0007	100	0.0835	0.0030	517	19

[a] D-TIMS values based on 27 grains analysed.
[b] ID-TIMS values based on 34 grains analysed. Both are from Heaman et al. [32].

epoxy mounts and ablation runs were conducted in raster mode using a much larger sample volume (45–60 μm × 60–100 μm). In addition, in a Pb–Pb isotope dating investigation of titanite by LA–MC–ICP-MS [30], the degree of Pb/U 'concordancy' for individual titanite grains was not evaluated and the grains were ablated in raster mode using extremely large sample volumes (500 μm × 1000 μm × 30 μm).

Large single crystals of titanite were isolated from the copper-mineralized pegmatite, at the Khan mine (Namibia) and used as an external standard. Kinny et al. [31] report an ID-TIMS concordant U–Pb age of 518 ± 2 Ma based on six analyses from splits of two crushed fragments. This age is in agreement with the titanite-K-feldspar isochron date of 521 ± 27 Ma (MSWD = 0.15) derived from the same sample material [31]. U–Pb ID-TIMS analyses of a separate Khan titanite sample yield a concordant age of 521.2 ± 2.4 Ma (Heaman et al., Unpublished data; Table 1), which is indistinguishable from the age reported by Kinny et al. [31].

At the start of a laser ablation session, analyses of the Khan titanite external standard were obtained using a 40 μm spot size, repetition rate of 4 Hz, and ∼3 J/cm^2 energy output. The Ar membrane gas flow rate for the DSN-100 was adjusted so as to produce a measured ^{206}Pb/^{238}U value essentially identical to the ID-TIMS value (Table 4). The laser ablation results for the Khan titanite are listed in Table 4 and shown in Fig. 4. The U–Pb data yield a concordant date of 516.9 ± 4.4 Ma, which is indistinguishable from the ID-TIMS ages reported in both Kinny et al. [31] and this study (Table 4). The data in Table 4 indicate that the Khan titanite grains analysed contain negligible (almost nil) common Pb. Upon completion of the standard analyses, the standard epoxy mount was replaced with the thin section to be analysed.

The analytical protocol developed here was verified using titanite from the Coldwell Complex, which represents the largest alkaline intrusion associated with the Midcontinent Rift System (MRS) in North America. Heaman and Machado [32] report

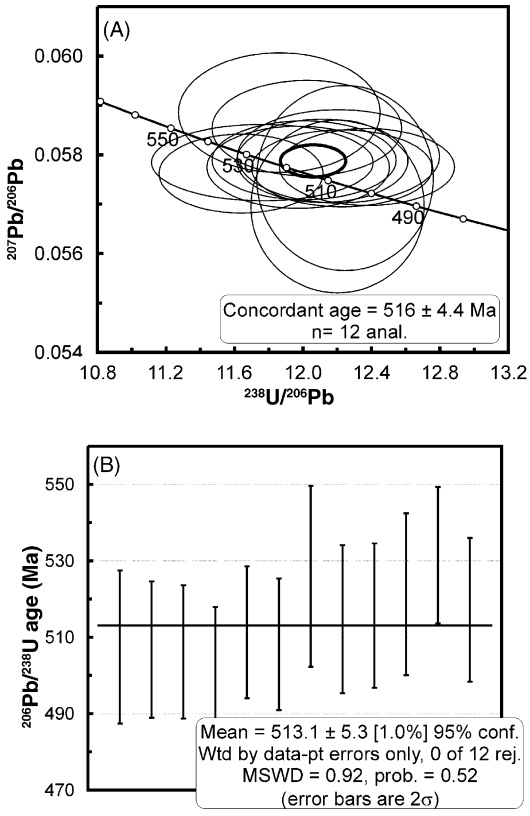

Fig. 4. Tera–Wasserburg diagram (A) and weighted average ^{206}Pb/^{238}U plot (B) for the laser ablation results (40 μm spot size) obtained for the Khan external titanite standard. Error ellipses in (A) are at 2σ levels.

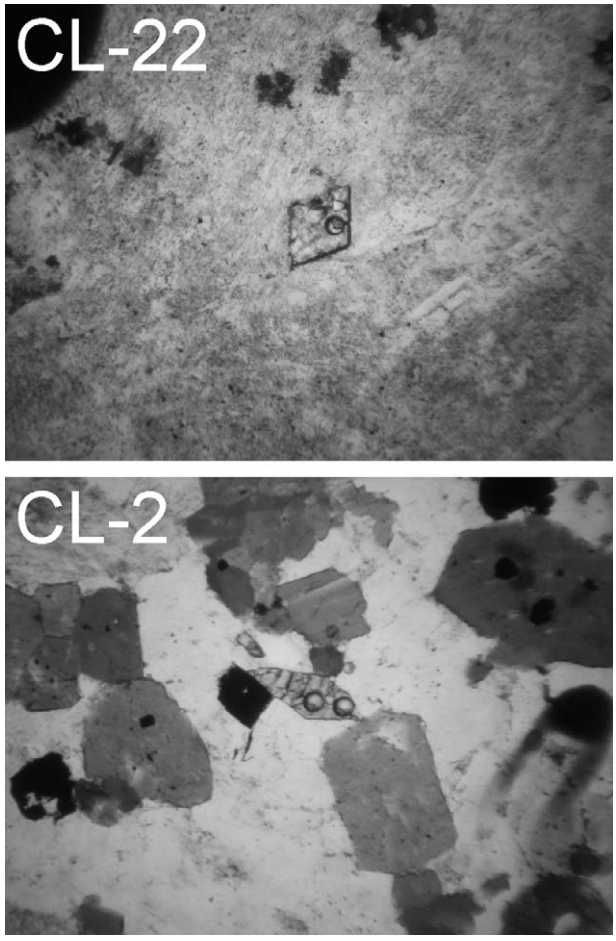

Fig. 5. Photomicrographs showing the location of 40 μm laser pits in petrographic thin sections of samples CL-22 (nepheline syenite) and CL-2 (granite).

a high precision zircon/baddeleyite U–Pb date of 1108 ± 1 Ma based on a detailed study of five samples from the Coldwell Complex. ID-TIMS dates were also determined on titanite from two samples, CL-2 (granite) and CL-22 (nepheline syenite) with ages of 1107 +9/−5 Ma and 1109 +8/−4 Ma, respectively [32]. In this study, we ablated titanite crystals from two thin sections, one from granite sample CL-2 and the other from nepheline syenite sample CL-22 (Fig. 5). Titanite crystals from the two thin sections were ablated using the same instrument parameters as those used for the concordant Khan titanite external standard. The titanite U–Pb laser ablation results are listed in Table 4 and shown on a Tera–Wasserburg plot and a weighted average ^{206}Pb/^{238}U diagram (Fig. 6). The LA–MC–ICP-MS analyses yield a lower intercept age of 1126 ± 19 Ma (2σ) in Fig. 6(A), and define a well-constrained mixing line between the radiogenic and common Pb components. Heaman and Machado [32] report common Pb isotope compositions for plagioclase, galena and K-feldspar from various magmatic phases associated with the Coldwell complex. These are fairly homogeneous with average ^{206}Pb/^{204}Pb, ^{207}Pb/^{204}Pb, and ^{207}Pb/^{206}Pb values of 16.31, 15.26, and 0.9355, respectively. The upper intercept associated with the regression line defined in Fig. 6(A) equates to a ^{207}Pb/^{206}Pb value of 0.7829 ± 0.30 for the common Pb component. This value is within the uncertainty of the average, initial ^{207}Pb/^{206}Pb value of 0.9355 ± 0.007 (2σ, standard deviation) obtained by ID-TIMS on several minerals from different phases of the Coldwell complex [32]. Thus, for the purposes of calculating the relative proportions of radiogenic versus common Pb in the titanite, the more accurate ID-TIMS value of ^{207}Pb/^{206}Pb = 0.9355 was used for the common Pb end-member, and the ^{207}Pb/^{206}Pb value of 0.07719 was taken for the radiogenic end-member (corresponds to age of lower intercept in Fig. 6(A)). The abundance of common Pb varies between <1 and 17% in titanite from granodiorite sample CL-2, and between 0.4 and 2.6% in titanite from nepheline syenite CL-22 (Table 4). The titanite data yield a weighted average ^{206}Pb/^{238}U age of 1120 ± 18 Ma (2σ; Fig. 6(B)). If a ^{207}Pb/^{206}Pb value of 0.7829 is taken (based on the graphical result) for the common Pb component, then the weighted average ^{206}Pb/^{238}U age becomes 1107 ± 21 Ma. Irrespective of the ^{207}Pb/^{206}Pb value that is assumed, both the lower intercept and weighted average ^{206}Pb/^{238}U ages are indistinguishable from the ID-TIMS ages obtained for several titanite fractions from samples CL-2 and CL-22 [32]. This result once again confirms the effectiveness of this analytical protocol in obtaining accurate and relatively precise (<2%, 2σ level) U–Pb dates for individual titanite grains in thin section.

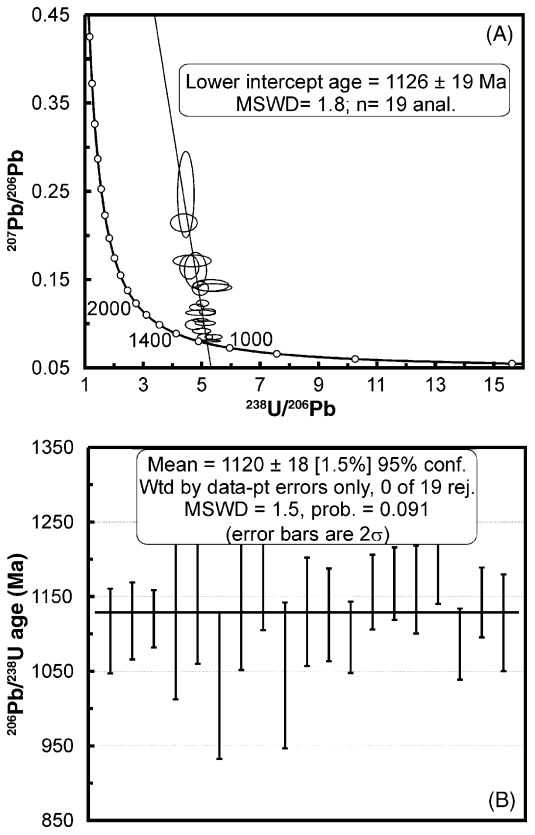

Fig. 6. Tera–Wasserburg diagram (A) and weighted average $^{206}Pb/^{238}U$ plot (B) for the laser ablation results (40 μm spot size) obtained for titanites within two thin sections (one for each) of samples CL-22 and CL-2. Error ellipses in (A) are at 2σ levels.

4. Summary and conclusions

In an earlier U–Pb study in our laboratory [3], the use of a 'standard-sample' bracketing technique during laser ablation analysis of standard and unknown grains within the same epoxy mount yielded a relative standard deviation (2σ; i.e., external reproducibility) of ≤3% and ≤1% for the Pb/U and $^{207}Pb/^{206}Pb$ values, respectively. We did not employ the same 'standard-sample' bracketing technique in this in situ U–Pb thin section dating study since it proved too cumbersome to embed grains of our mineral standards into the thin sections. However, to test the stability of the Pb/U normalization procedure used here, the epoxy standard mount was re-inserted into the ablation cell for re-analysis at the end of the day during several analytical sessions. In each case, the Pb/U normalization values were determined to have remained constant or within the relative standard deviation of the method. The lack of a significant change in the LIEF for the Pb/U values greatly increases the capacity for sample through-put in that a much larger segment of the analytical session can be spent in analyzing unknown rather than standard grains. The LIEF affects solely the measured Pb/U since the Pb/Pb ratios are always simultaneously corrected for instrumental mass bias with the nebulized thallium solution aspirated through the DSN-100. Small inaccuracies in the Pb/U values (and associated normalization factors) will simply cause the data to slide 'up or down' along their corresponding $^{207}Pb/^{206}Pb$ lines. Possible causes for the change in Pb/U values related to instrument conditions include a variable solution uptake rate associated with the Meinhardt nebulizer (on the DSN-100), or rapidly decreasing backing pressure in the main Ar gas line during an analytical session. Thus, at the very least, the laser ablation U–Pb data obtained in situ from thin sections should yield accurate $^{207}Pb/^{206}Pb$ values (and ages) and should be within analytical uncertainty of those determined by ID-TIMS.

Of greater concern in comparing LA–MC–ICP-MS and ID-TIMS results is with regard to grain selection. ID-TIMS analyses are generally conducted on the 'best quality' grains, which are selected after extensive mineral separation steps followed in some cases by removal of damaged areas by physical or chemical abrasion. This approach optimizes the chances of obtaining concordant age data but may bias ages towards a particular population of grains. In contrast, analysis of all available grains of a particular accessory mineral in a thin section by LA–MC–ICP-MS may provide a more representative indication of age populations in the sample but will likely result in the analysis of more discordant grains. In our experience, discordancy can be mitigated to some degree through back-scatter electron imaging of grains prior to analysis (e.g., Fig. 3(D)), which enables the selection of optimal analysis spots on individual grains that are homogeneous and devoid of imperfections.

The U–Pb laser ablation results obtained here for zircon, monazite and titanite grains in standard petrographic thin sections demonstrate the effectiveness of this technique in providing accurate and relatively precise age information. One of the main advantages of this technique is that it is relatively rapid and requires minimal sample preparation. It should prove particularly valuable for obtaining U–Pb ages in reconnaissance-type studies, such as preliminary geological studies of regions that contain little or no prior geochronological age information. This technique is also capable of in situ dating of tiny U-bearing mineral inclusions (e.g., monazite inclusions in garnet) and will provide important contextual age information. Geochronological analysis of accessory minerals in thin sections is a cost effective tool for 'pre-screening' optimal samples to be dated by more labour-, time- and cost-intensive ID-TIMS (and possibly SHRIMP) analysis. The analytical protocol presented here cannot substitute for the higher precision dates obtained by ID-TIMS, but at the very least it should serve as a reliable, complimentary geochronological tool.

The results reported here clearly indicate that this technique uses much less sample volumes but can routinely provide uncertainties on age determinations that are equivalent to or better than those reported using quadruple ICP-MS or MC–ICP-MS instruments equipped with an all Faraday collector array [e.g., Refs. 2,7]. For example, U–Pb laser ablation analyses of monazite conducted here using a spot size of 5 μm (pit depth of ∼2 μm) consumes ∼1000 times less sample volume (and corresponding total Pb consumed) compared to previous LA–MC–ICP-MS analysis of monazite using a 'rastering' technique [1]. The use of such a large raster area (60 μm × 60 μm × 15 μm) for routine U–Pb geochronological investigations of accessory minerals in petrographic thin sections would not be feasible for the majority

of the grains investigated in this study. In addition, the larger volumes of material sampled by raster mode analyses make it more difficult to directly date distinct age domains within relatively small (<100 μm) individual grains (e.g., Fig. 3(B) and (D)).

Acknowledgements

The radiogenic isotope facility at the University of Alberta is supported by a NSERC Major Facility Access grant. We thank GuangCheng Chen for his assistance and technical support provided during the course of this study. We thank D. Resultay and M. Labbe for help preparing the standard blocks and thin sections. We thank J. Košler and an anonymous reviewer for their insightful comments.

References

[1] M.S.A. Horstwood, G.L. Foster, R.R. Parrish, S.R. Noble, G.M. Nowell, J. Anal. Atom. Spectrom. 18 (2003) 837.
[2] S.E. Jackson, N.J. Pearson, W.L. Griffin, E.A. Belousova, Chem. Geol. 211 (2004) 47.
[3] A. Simonetti, L.M. Heaman, R.P. Hartlaub, R.A. Creaser, T.G. MacHattie, C.O. Böhm, J. Anal. Atom. Spectrom. 20 (2005) 677.
[4] M. Bizzarro, A. Simonetti, R.K. Stevenson, J. David, Geology 30 (2002) 771.
[5] S.S. Schmidberger, L.M. Heaman, A. Simonetti, R.A. Creaser, H.O. Cookenboo, Earth Sci. Planet. Lett. 240 (2005) 621.
[6] R.P. Hartlaub, T. Chacko, L.M. Heaman, R.A. Creaser, K.E. Ashton, A. Simonetti, Precambrian Res. 141 (2005) 137.
[7] C.M. Valeriano, N. Machado, A. Simonetti, C.S. Valladares, H.J. Seer, L.S.A. Simões, Precambrian Res. 130 (2004) 27.
[8] P. Bence, J.D. Woodhead, J. Hergt, J. Anal. Atom. Spectrom. 20 (2005) 1350.
[9] T.E. Jeffries, J. Fernandez-Suarez, F. Corfu, G. Guitierrez-Alonso, J. Anal. Atom. Spectrom 18 (2003) 847.
[10] G. Foster, R.R. Parrish, M.S.A. Horstwood, S. Chenery, J. Pyle, H.D. Gibson, Earth Planet. Sci. Lett. 228 (2004) 125.
[11] A. Zeh, I.L. Millar, M.S.A. Horstwood, J. Petrol. 45 (2004) 949.
[12] W. Todt, R.A. Cliff, A. Hanser, A.W. Hofmann, Geophys. Mongr. Am. Geophys. Union 95 (1996) 429.
[13] R.N. Taylor, T. Warneke, J.A. Milton, I.W. Croudace, P.E. Warwick, R.W. Nesbitt, J. Anal. Atom. Spectrom. 18 (2003) 480.
[14] S. Chenery, J.M. Cook, J. Anal. Atom. Spectrom. 8 (1993) 299.
[15] D. Günther, H. Cousin, B. Magyar, I. Leopold, J. Anal. Atom. Spectrom. 12 (1997) 165.
[16] I. Horn, R.L. Rudnick, W.F. McDonough, Chem. Geol. 164 (2000) 281.
[17] S.M. Eggins, L.P.J. Kinsley, J.M.G. Shelley, Appl. Surf. Sci. 127–129 (1998) 278.
[18] L.P. Dunstan, J.W. Gramch, I.L. Barnes, W.C. Purdy, J. Res. Natl. Bur. Stand. 85 (1980) 1.
[19] R. Stern, Y. Amelin, Chem. Geol. 197 (2003) 111.
[20] K.E. Ashton, L.M. Heaman, J.F. Lewry, R.P. Hartlaub, R. Shi, Can. J. Earth Sci. 36 (1999) 185.
[21] K.R. Ludwig, US Geological Survey Revision of Open-File Report 91-445, 1994.
[22] L.M. Heaman, R.H. McNutt, T.E. Krogh, Geol. Assoc. Can. Spec. Paper 31 (1986) 209.
[23] A.J.G. Mank, P.R.D. Mason, J. Anal. Atom. Spectrom. 14 (1999) 1143.
[24] D.J. Cherniak, E.B. Watson, M. Grove, T.M. Harrison, Geochim. Cosmochim. Acta 68 (2004) 829.
[25] M.D. Schmitz, S.A. Bowring, Geol. Soc. Am. Bull. 115 (2003) 533.
[26] D. Bosch, D. Hammor, O. Bruguier, R. Caby, J.-M. Luck, Chem. Geol. 184 (2002) 151.
[27] F. Tera, G.J. Wasserburg, Earth Planet. Sci. Lett. 14 (1972) 281.
[28] W. Compston, I.S. Williams, C.E. Meyer, J. Geophys. Res. B89 (1984) 525.
[29] C.D. Storey, T.E. Jeffries, M. Smith, Chem. Geol. 227 (2006) 37.
[30] B.J.A. Willigers, J.A. Baker, E.J. Krogstad, D.W. Peate, Geochim. Cosmochim. Acta 66 (2002) 1051.
[31] P.D. Kinny, N.J. McNaughton, C.M. Fanning, R. Maas, U.S. Geol. Surv. Circular 1107 (1994) 171.
[32] L.M. Heaman, N. Machado, Contrib. Mineral. Petrol. 110 (1992) 289.
[33] K.R. Ludwig, Berkeley Geochronological Center Spec. Publ. no. 4, 2003.